Lidar Multiple Scattering Determinations of Particle Size in Cirrus Clouds

Edwin W. Eloranta and Ralph E. Kuehn *University of Wisconsin-Madison, 1225 W. Dayton St., Madison WI 53706, e-mail: eloranta@lidar.ssec.wisc.edu*

Basic Approach

HSRL measurements of backscatter cross section provide the projected area of particles per unit volume as viewed from the lidar.

+

HSRL measurements of multiple scattering provide information on the shape of the diffraction peak. The angular width is directly related to the cross-sectional area of individual particles.

+ Radar provides the 6th moment of the size distribution when used with the lidar cross section. → Provides two parameters describing the projected area particle size distribution → Doppler radar measurements of particle fall velocity + Drag force relationship with assumption about the drag coefficient → Provides ice water mass

Provides two parameters describing the projected area particle size distribution → Assumed projected area volume relationship → Provides ice water mass

+ Assumed projected area volume relationship → Provides ice water mass

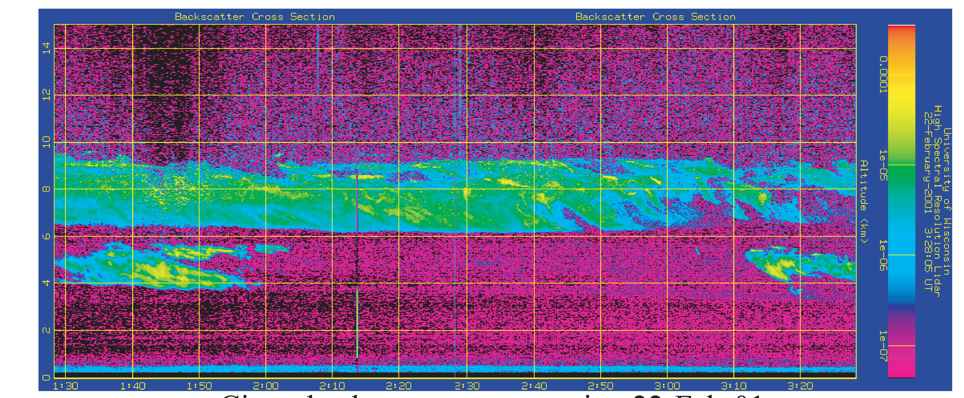
Cirrus backscatter cross section 22-Feb-01

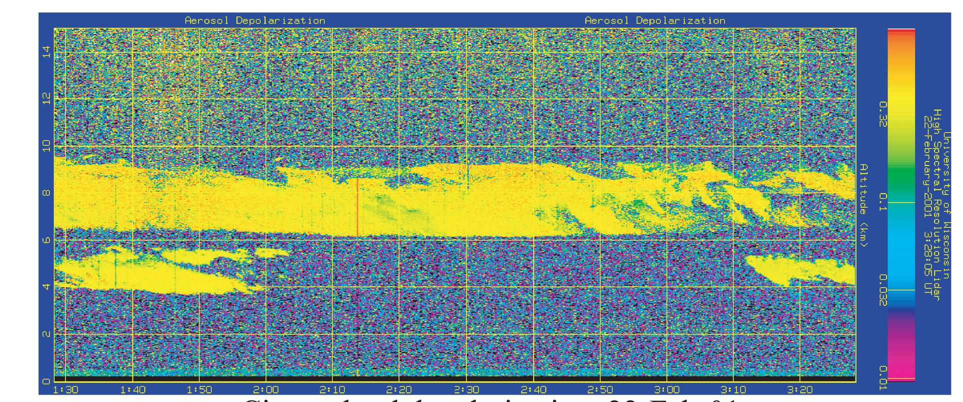
Cirrus cloud depolarization, 22-Feb-01

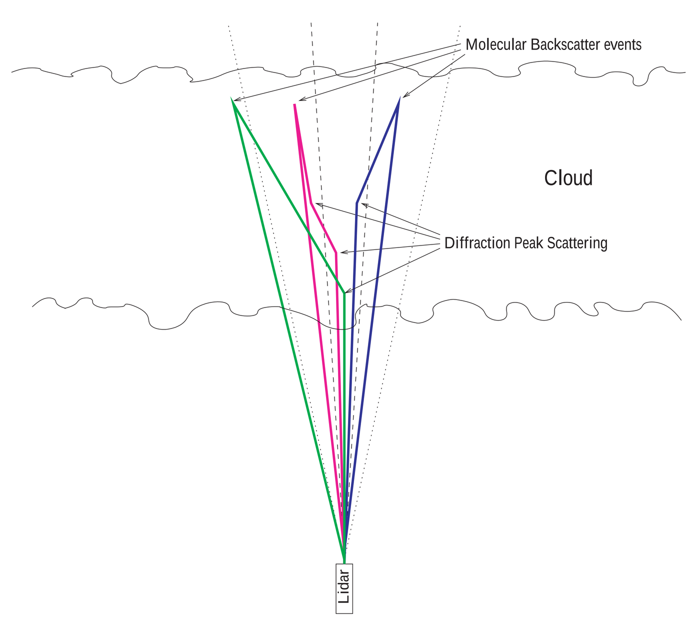

HSRL multiple field of view measurements and a multiple scattering model provide information on forward diffraction peak of the scattering phase function. This is used to derive particle size distribution parmeters. This distribution describes the dimensions of particles projected on a plane perpendicular to the lidar beam. The HSRL is able to isolate photons which have undergone one or more small angle forward scatterings coupled with one molecular backscatter event.

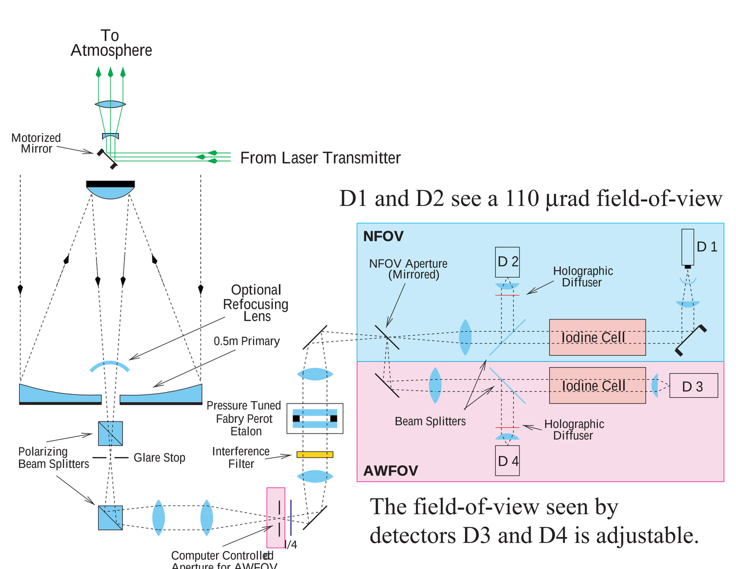

HSRL Receiver Schematic. Gieger-mode APD (D1), and wide-field-of-view channels have been made operational under this grant. The APD has provided a factor of 10 improvement in the sensitivity of this channel.

Exponential Distribution

$$\frac{dn}{dr} = a\ \exp(-br)$$

$$b = \frac{3}{r_{eff}}$$

Optical-radar radius effective radius

$$<r> = 1.45\ r_{eff}$$

Optical-radar radius

$$<r> = \sqrt[4]{\frac{<r^6>}{<r^2>}}$$

Log-Normal Distribution

$$\frac{dn}{dr} = \frac{a}{\alpha r}\exp\left[-\frac{1}{2}\left(\frac{\ln\left(\frac{r}{\alpha}\right)}{\gamma}\right)^2\right]$$

$$\alpha = r_{eff}\ \exp(-2.5\gamma^2)$$

Optical-radar radius effective radius

$$<r> = r_{eff}\ \exp(1.5\ \gamma^2)$$

Gamma Distribution

$$\frac{dn}{dr} = a\ r^{\alpha}\ \exp(-b\ r^{\gamma})$$

$$b = \left(\frac{1}{r_{eff}}\frac{\Gamma\left(\frac{\alpha+4}{\gamma}\right)}{\Gamma\left(\frac{\alpha+3}{\gamma}\right)}\right)^{\gamma}$$

Optical-radar radius effective radius

$$<r> = r_{eff}\ \frac{\Gamma\left(\frac{\alpha+3}{\gamma}\right)}{\Gamma\left(\frac{\alpha+4}{\gamma}\right)}\left(\frac{\Gamma\left(\frac{\alpha+7}{\gamma}\right)}{\Gamma\left(\frac{\alpha+3}{\gamma}\right)}\right)^{\frac{1}{4}}$$

Changes in lidar multiple scattering caused by changing the shape of the size distribution. Mulitple scattering was computed using the scattering cross section profile measured on 22-Feb-01 with the effective radius fixed at 75 microns. The sum of 2nd and 3rd order scattering divided by first order scattering is shown for each size distribution and each receiver field-of-view. Size distributions are designated by color.

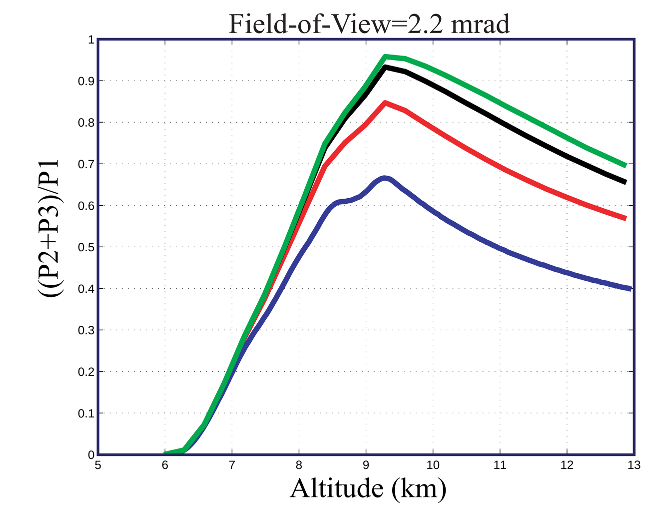

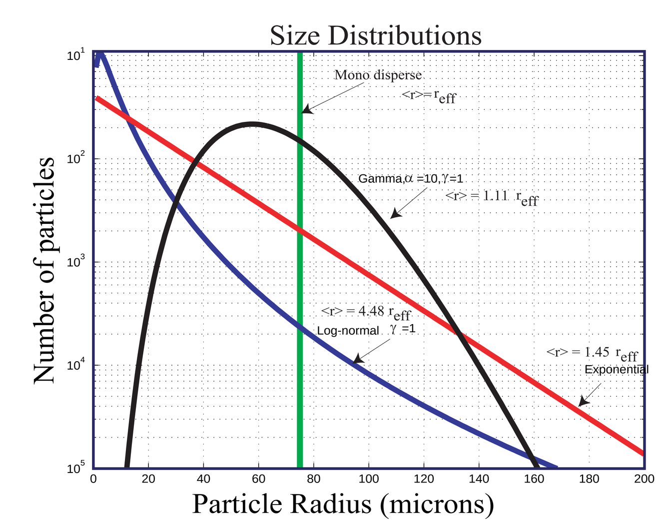

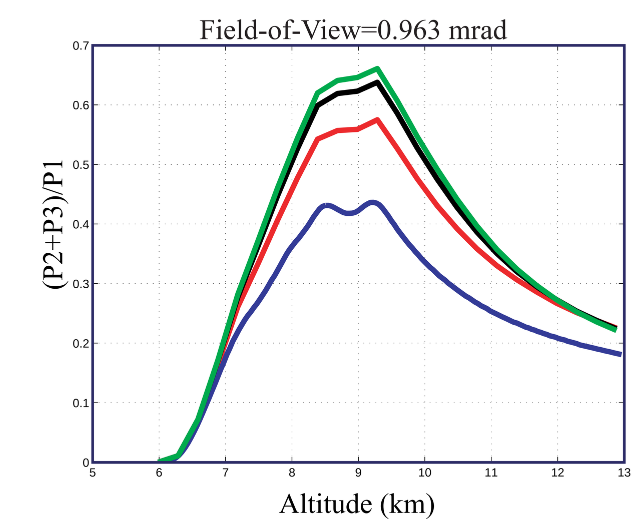

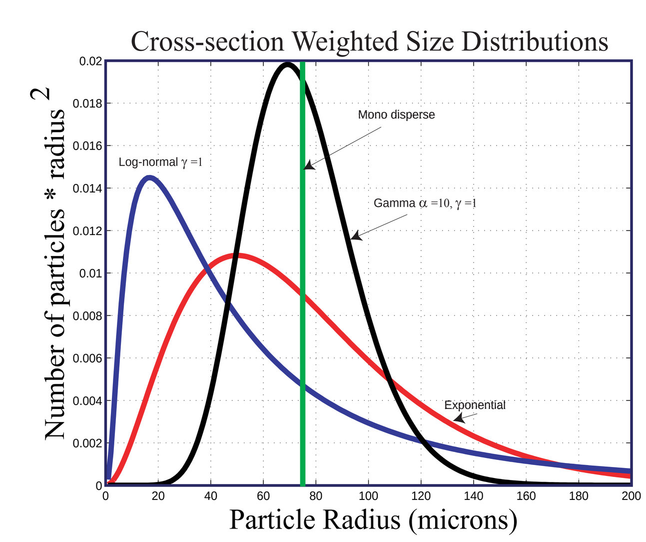

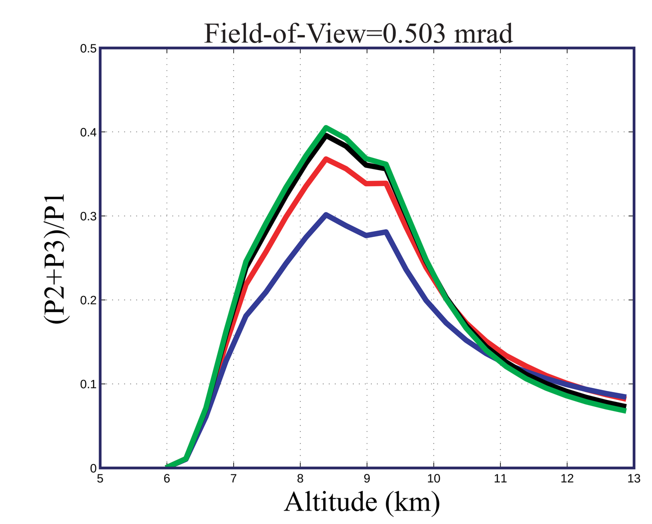

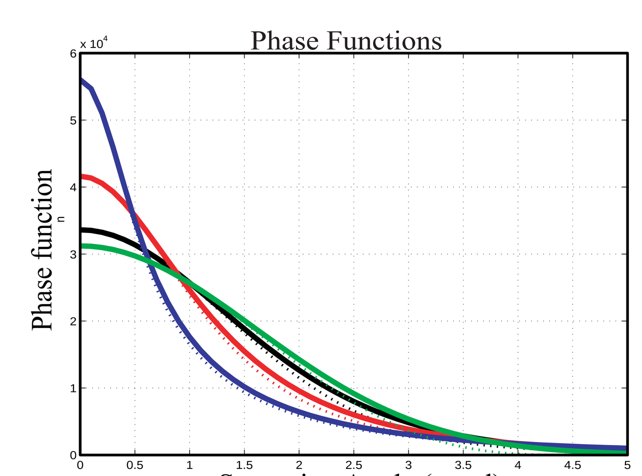

A comparison of the phase functions for the different size distributions using the Gaussian approximation (Solid lines), and using diffraction theory (dashed lines).

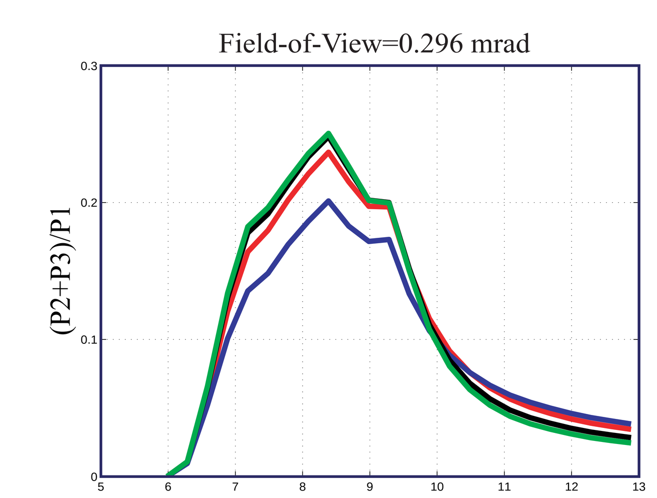

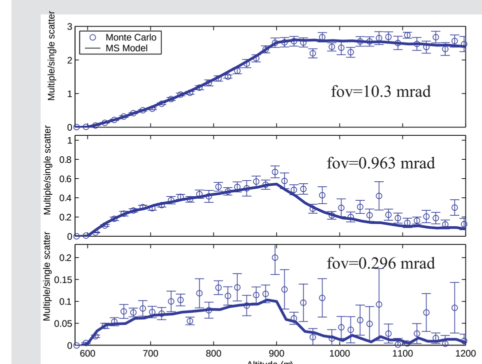

A comparison between the multiple-to-single scatter ratios predicted by the Gaussian multiple scatter model (solid lines) and a Monte Carlo simulation of 96 billion photon trajectories (points).

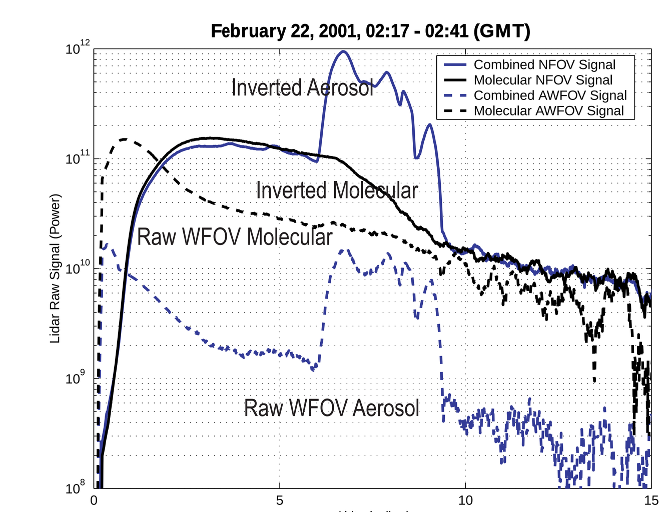

Measured Lidar returns.

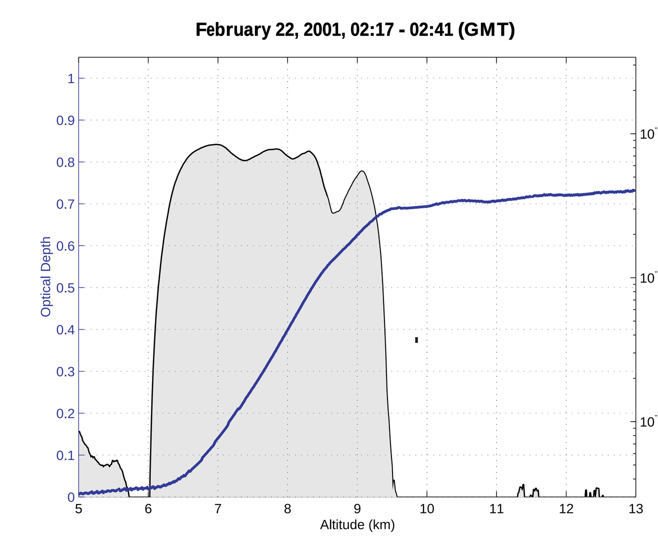

Optical depth and backscatter cross section.

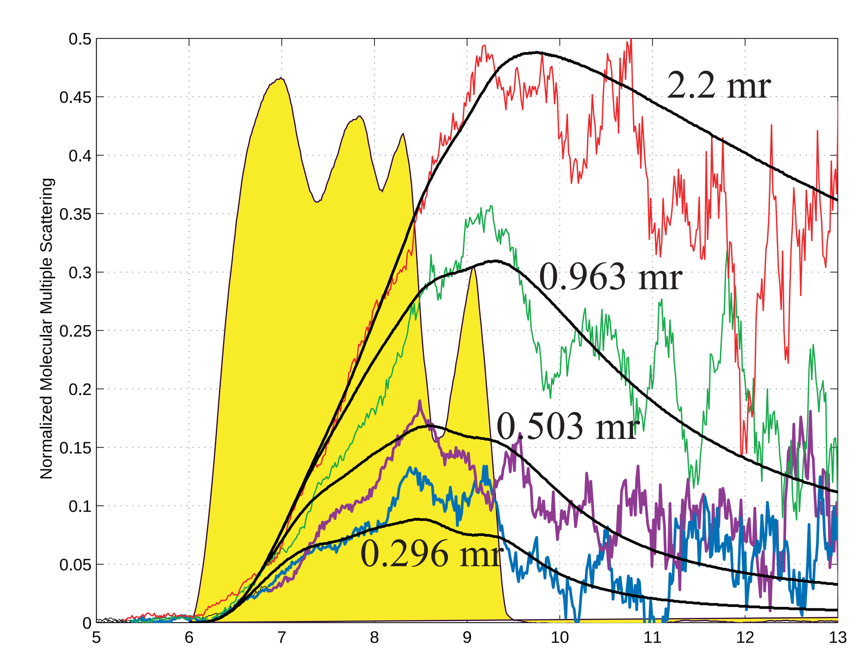

A comparison of the measured multiply scattered molecular lidar return (colored lines) and the model predictions (solid black lines) using r_{eff} =75 microns and $\gamma = 0$. The backscatter cross section is shown in yellow.

Our wide field of view measurements are presented in terms of a normalized return =

$$\frac{\text{WFOV signal-k*(110 urad FOV molecular signal)}}{\text{(110 urad FOV molecular signal)}}$$

Where: $k = \dfrac{\text{Clear air WFOV Signal}}{\text{Clear air 110 urad FOV signal}}$

and where WFOV is the molecular wide-field of view channel.

We have derived multiple scatter lidar equations describing the ratio of nth order multiple scattering to first order scattering as a function of range (R) for several mathematical models of the particle size distribution. These equations assume :

1) Particle sizes described by log-normal, exponential, gamma or mono disperse distributions.
2) Particles that are large compared to the lidar wavelength, λ.
2) A Gaussian distribution of energy in the transmitted beam with an angular width = $2\rho_l$.
3) A receiver field-of-view = $2\rho_t$.
4) A backscatter phase function $P(\pi,R)$ with an average value of $P_{n\pi}(R)$ for angles near π.
5) A cloud optical depth = $\tau(R)$, scattering cross section = $\beta(R)$

For the log-normal distribution:

$$\frac{P_n(R)}{P_1(R)} = \frac{P_{n\pi}(R)}{P(\pi,R)}\left[1-\exp(-\frac{\rho_t^2}{\rho_l^2})\right]^{-1}\left\lfloor\frac{\tau^{n-1}}{(n-1)!}-\int_{z_c}^{R}\frac{\beta(z_1)}{\sqrt{\pi}}\int_{-\infty}^{\infty}\exp(-u^2)\cdots\int_{z_{n-2}}^{R}\frac{\beta(z_{n-1})}{\sqrt{\pi}}\int_{-\infty}^{\infty}\exp(-u^2)\exp\left(\frac{-\pi^2\rho_t^2R^2/\lambda^2}{(R-z_1)^2\left(\frac{\exp(-\sqrt{2}\gamma(z_1)u_1-2\gamma(z_1)^2)}{\alpha(z)}\right)+\cdots(R-z_{n-1})^2\left(\frac{\exp(-\sqrt{2}\gamma(z_{n-1})u_{n-1}-2\gamma(z_{n-1})^2)}{\alpha(z)}\right)+\pi^2\rho_l^2R^2/\lambda^2}\right)du'_{n-1}dz_{n-1}du'_{n-2}dz_{n-2}...du'_1dz_1\right]$$

For the gamma distribution:

$$\frac{P_n(R)}{P_1(R)} = \frac{P_n(\pi,R)}{P(\pi,R)}\left[1-\exp(-\frac{\rho_t^2}{\rho_l^2})\right]^{-1}\left[\frac{\tau^{n-1}}{(n-1)!}-\int_{z_c}^{R}\beta(z_1)\frac{\gamma(z_1)}{\Gamma\left(\frac{\alpha(z_1)+3}{\gamma(z_1)}\right)}\int_0^{\infty}u(z_1)^{\alpha(z_1)+2}\exp(-u(z_1)^{\gamma(z_1)})...\int_{z_{n-1}}^{R}\beta(z_{n-1})\frac{\gamma(z_{n-1})}{\Gamma\left(\frac{\alpha(z_{n-1})+3}{\gamma(z_{n-1})}\right)}\int_0^{\infty}u(z_{n-1})^{\alpha(z_{n-1})+2}\exp(-u(z_{n-1})^{\gamma(z_{n-1})})\exp\left(-\frac{\pi^2\lambda^{-2}\rho_t^2R^2}{(R-z_1)^2\left(\frac{1}{u(z_1)}\frac{1}{r_{eff}(z_1)}\frac{\Gamma\left(\frac{\alpha(z_1)+4}{\gamma(z_1)}\right)}{\Gamma\left(\frac{\alpha(z_1)+3}{\gamma(z_1)}\right)}\right)^2+...(R-z_{n-1})^2\left(\frac{1}{u(z_{n-1})}\frac{1}{r_{eff}(z_{n-1})}\frac{\Gamma\left(\frac{\alpha(z_{n-1})+4}{\gamma(z_{n-1})}\right)}{\Gamma\left(\frac{\alpha(z_{n-1})+3}{\gamma(z_{n-1})}\right)}\right)^2+\pi^2\lambda^{-2}\rho_l^2R^2}\right)du_{n-1}dz_{n-1}...du_1dz_1\right]$$

μm

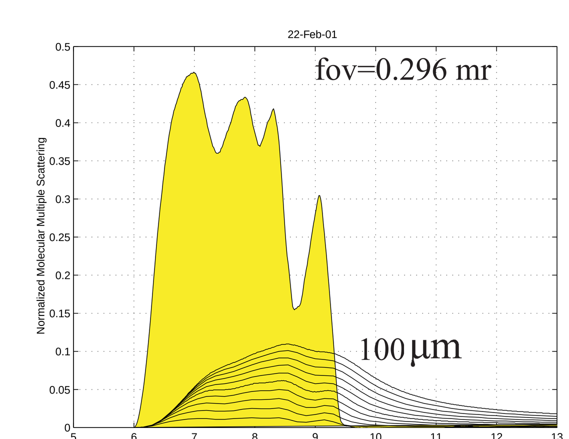

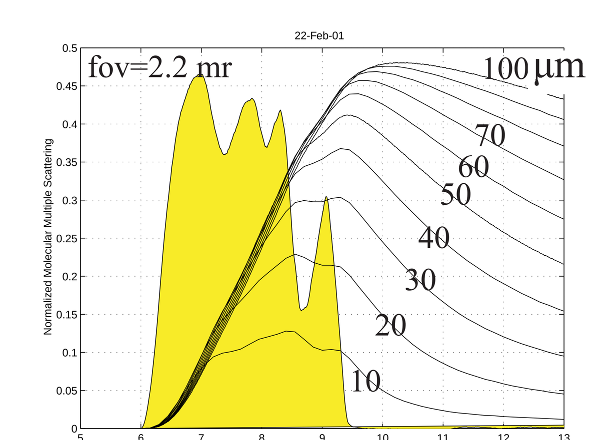

The normalized molecular wide field of view lidar return computed as function of receiver field of view and r-eff with $\gamma = 0$. The backscatter cross section profile of the cloud is shown in yellow (relative units).